



# Experimental analysis on tensile strengthening properties of steel and glass fiber reinforced inorganic matrix composites

H. Jahangir and M.R. Esfahani\*

*Department of Civil Engineering, Ferdowsi University of Mashhad, Mashhad, P.O. Box 9177948974, Iran.*

Received 8 November 2019; received in revised form 28 May 2020; accepted 16 November 2020

## KEYWORDS

Fiber-Reinforced  
Inorganic Matrix  
(FRIM) composites;  
Steel fibers;  
Glass fibers;  
Inorganic lime mortar;  
Inorganic geopolymer  
mortar;  
Failure modes.

**Abstract.** The Fiber-Reinforced Inorganic Matrix (FRIM) composite is a new type of composite, which has many economical and performance advantages. Beside the direct shear and bending tests, the tensile tests form an integral part in determining the mechanical properties of these composites. In this paper, to understand the tensile behavior of the FRIM composites, some strip specimens of the composites were tested which were clamped at both ends, and the strains were measured using the extensometers installed at the middle of each strip. The inorganic matrix composites studied in this paper were constructed using two types of steel and glass fibers together with two different types of inorganic lime and geopolymer mortars. The results of direct tensile tests showed that the inorganic geopolymer mortars had the higher potential to increase the tensile load bearing of the specimens compared with the lime mortars. In addition, in most cases, the maximum values of stress, strain and the stiffness at the final stage of response in the tensile tests of composites were consistent with the results reported from the tensile test of textile fibers without the mortar. Moreover, clamping specimens by applying sufficient compressive force prevents slipping of fibers within the surrounding mortar.

© 2021 Sharif University of Technology. All rights reserved.

## 1. Introduction

Fiber-reinforced composite systems play an important role in providing strengthening goals, including the reduction of construction costs, increase in the service life of structures, and prevention of damage induction and development [1]. The Fiber-Reinforced Inorganic Matrix (FRIM) composite is a new type of composite, which is a suitable and efficient replacement for Fiber-Reinforced Polymers (FRPs). The fibers in FRIM

composites are normally interwoven, and inorganic materials are used instead of epoxy adhesive as the matrix. Inorganic materials can be used as the matrix of FRIM systems due to their properties and capabilities, such as high thermal resistance, resistance to ultraviolet radiation, low radiation during production and installation, and good experience with correct usage [2]. The efficiency of FRIM composites depends on factors such as the bond between the fibers and the inorganic matrix, the capability of the inorganic matrix to completely coat the inside fiber strands, the bond between FRIM composite and the substrate, the bond between the longitudinal and transverse fibers, and the cracking of inorganic matrix [3]. In addition, the inadequate ability of the inorganic matrix to penetrate through the fiber strands and the void spaces, and also

\*. Corresponding author. Tel.: +98 513 8673716  
E-mail addresses: jahangir.hashem@mail.um.ac.ir (H. Jahangir); esfahani@um.ac.ir (M.R. Esfahani)

the weak transfer of shear force between them, can lead to uneven distribution of the tensile stress in the fibers, followed by non-uniform failure [4].

To understand the mechanism of interfacial stress transfer in inorganic matrix composites, in addition to the shear [5–9], bending [10–13] and torsion [14] tests, tensile tests are an integral part of determining the mechanical properties of these composites. Tensile tests can be used for various fiber and matrix combinations and meet the design requirements of FRIM composites. Due to the interaction of the fibers and the surrounding matrix, the mechanical properties derived from the experiments separately performed on the fibers and the matrix cannot directly be used to obtain the properties of their produced composite [15]. Because of such interaction, some cracks are developed in the matrix, and slip sometimes occurs between the fibers and the surrounding matrix. The characteristics of tensile tests on inorganic matrix composites can play a decisive role in their axial stress-strain behavior [15].

Finding an efficient and common test method for testing FRIM composites in tension is of particular importance due to the presence of various materials and combinations of the fiber-matrix. Previous studies have reported many problems in determining the characteristics of FRIM composites [16]. Although various tensile test devices have been used and many researchers have proposed various suggestions, there is still no common approach to the tensile test of FRIM composites [17–20]. The fundamental differences of various test devices are in the configuration of specimens, the clamping method at the beginning and end of the specimen, and measurement methods. The most common specimens in tensile tests are rectangular [17,21–24] and dumbbell [25–28] strips, with or without an increase in thickness at both ends of the specimen. The methods for restraining the rectangular strip specimens in the tensile test device are undertaken by means of hydraulic or pneumatic clamps [22,29], steel plates bolted to the specimen [17,30,31], attaching the steel or aluminum plates to both ends of the specimen and bolting the plates to the test device [32–35], and making holes at both ends of the specimen and passing the steel bars [36–38]. The dumbbell specimens are typically restrained in the tensile test device using the steel clamps of the test device adjusted with the curvature radius of the specimen. There are rubber sheets between the steel clamps and the specimen to prevent stress concentration between the steel plates and the composite matrix. The displacements during the tensile test can be measured using the test device clamps [39], Linear Variable Displacement Transducers (LVDTs) or extensometers placed on the specimen [40], employing imaging technology [35,41] and fiber optics [42,43].

Different tensile test devices can be evaluated

using different monitoring methods. Although the tensile tests were performed on the polymer-based composites with force control [44], most tensile tests are conducted on inorganic matrix composite specimens with displacement control, and an increase in the spacing of the device clamps at a specified rate. Kim et al. [45] evaluated the effect of loading rate on the tensile behavior of FRIM composites. The results of the study showed that maximum axial stress and the cracking pattern of specimens are strongly dependent on the loading rate.

Each of the direct tensile test devices has its own advantages and disadvantages, and the results obtained from different test devices can vary. The tests performed on the rectangular strip specimens with two different clamping methods show that the obtained results are very different and are strongly dependent on the test device and the methodology [46]. Recently, Al-Gemeel et al. [47] studied ring-shaped specimens to evaluate the apparent loop tensile load. In general, the results obtained from the tensile tests on inorganic matrix composites are affected by the presence of bending moments inside and outside the specimen plate, defects during the construction, and the measurement method used [48]. Donnini et al. [49] analyzed the effect of overlapping the bidirectional glass fiber networks on the tensile behavior of FRIM composites. They used Digital Image Correlation (DIC) technology to measure the axial displacements in the laboratory specimens, with variable overlapping lengths of 100–200 mm. In addition, various factors, such as the geometry and construction process of the textile fiber, the cross-section of fiber strands, degree of continuity between the longitudinal and transverse fibers in the network fabric, affect the results of the tensile test, which requires further research despite numerous amounts of work done in this field.

In this paper, the tensile behavior of inorganic matrix composites with steel, as a newly developed kind of fiber, and glass fibers are investigated to understand the tensile behavior of inorganic matrix composites. The steel-fiber composites were coated with two types of inorganic lime and geopolymer mortars, and the glass-fiber composites were only coated with the inorganic lime mortars to be more consistent. To prevent the fibers from slipping into the surrounding mortar, the specimens were clamped on the mortar by applying adequate compressive force from the device strokes. The axial strains were measured by the device strokes and also the extensometers placed in the middle of the specimen on the surface of the specimen.

## 2. Ideal response of axial stress-strain

Although different inorganic matrix composites with various fibers and matrices have different tensile behav-

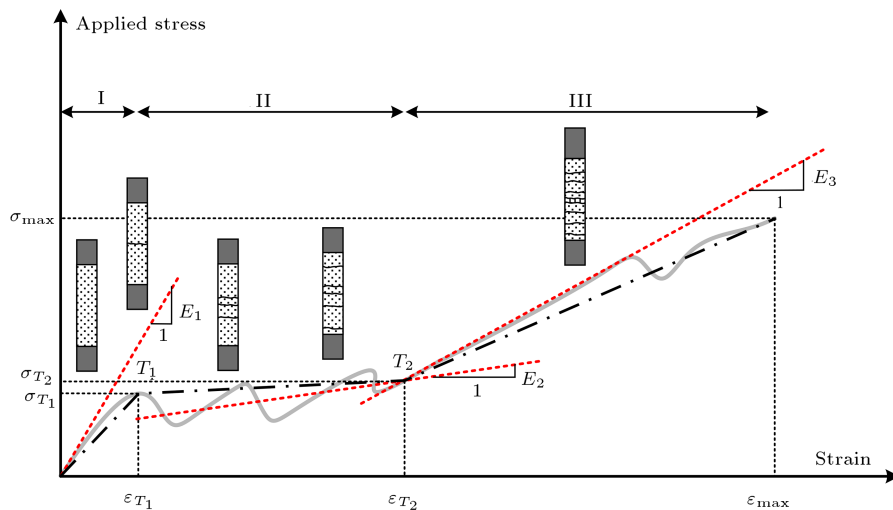


Figure 1. Ideal stress-strain response of inorganic matrix composite in tensile test [51].

ior, according to previous studies [50,51] and as shown in Figure 1, an ideal response can be presented for the axial stress-strain curves of these composites [51].

Generally, the ideal trilinear stress-strain behavior should not depend on the test device. However, in reality, the specimen geometry, volume ratio of fibers along the network, clamping method, and test controlling methodology can influence the test results. Based on the ideal stress-strain response presented in Figure 1, the behavior of the specimen is linear and elastic before the matrix is cracked. This stage, considered as the first stage and called the ‘without cracking’ stage, ends with the development of the first crack in the matrix, which is, in most cases, associated with a sudden drop in stress. By increasing the displacement, more cracks occur along the specimen, and as a result, the axial stresses are not significantly increased. This is called the second stage or the crack development stage in the tensile behavior of the inorganic matrix composites. When no new crack appears in the composite matrix and the crack saturation state occurs, the third stage begins, where the load is solely applied to the longitudinal fibers of the specimen. Hence, the slope of the response at the third stage should be consistent with the elasticity modulus of the fiber network and, as expected, the failure of the specimen should also occur due to the rupture of the fibers.

In some cases, the rupture of the fibers in the second stage may occur concurrently with the development of cracks in the composite inorganic matrix, and may reduce composite stiffness relative to the axial stiffness of the fibers without the surrounding coating at the third stage. In addition, based on the test device intended for the composite tensile test, the fibers may slip between the composite surrounding matrix at the second and third stages. In this case, the rupture

possibility of the fibers is decreased, and the third stage will end with the slip of the fibers. Moreover, usually, when both the fiber and the mortar are gripped and the tensile load applied, cracks occur in the clamp area and the mortar pulls out from the fiber. As a result, for some composites with a low-strength inorganic matrix and a slip of fibers within the matrix, the second stage of the response cannot be distinguished from the third stage [33]. It should be noted that the absence of the second stage of the tensile stress-strain response in some of the high-strength inorganic matrix composites, large volume ratio of fibers, and an appropriate bond between the fibers and the matrix are also observed [52]. The axial stress-strain behavior of such composites will be bilinear.

Based on the ideal trilinear response shown in Figure 1, the tensile stress-strain curves of inorganic matrix composites can be obtained by nine parameters, including the stresses  $\sigma_{T1}$ ,  $\sigma_{T2}$  and  $\sigma_{max}$ , corresponding strains  $\varepsilon_{T1}$ ,  $\varepsilon_{T2}$  and  $\varepsilon_{max}$  and slopes of the first, second and third stages,  $E_1$ ,  $E_2$  and  $E_3$ , respectively. The stress  $\sigma_{T1}$  and the corresponding strain  $\varepsilon_{T1}$  from the intersection point of the first and second stages, point  $T_1$ , are obtained simultaneously with the occurrence of the first crack in the specimen. The stress  $\sigma_{T2}$  and the corresponding strain  $\varepsilon_{T2}$  from the intersection point of the second and third stage, point  $T_2$ , are simultaneously determined as the linear behavior of the response has begun after the saturation of the cracks in the composite matrix. The specimen failure is identified with the ultimate stress  $\sigma_{max}$  and the corresponding strain  $\varepsilon_{max}$ . The stresses can be calculated based on the overall cross-section of the composite, including the fibers and matrix or based on the cross-section of the longitudinal fibers.

Since it is not always straightforward to achieve these nine parameters, curve fitting methods can be

used. Because of the nonlinear behavior of the tensile stress-strain curve, the slope of different stages for determining  $E_1$ ,  $E_2$ , and  $E_3$  may be different with the slope of the lines considered for creating the ideal trilinear response. In fact, the first stage begins linearly in some inorganic matrix composites, but becomes nonlinear before the first crack occurs. This nonlinear behavior can be caused by the development of micro-cracks that eventually develop into the first crack in the specimen. In this case, the  $E_1$  parameter represents the slope of the curve in the linear branch of the first stage. The slope of the cracking stage, second stage, is obtained by fitting the curve between points  $T_1$  and  $T_2$ , which is normally different from the linear curve slope between these two points. When the occurrence of the first crack in the specimen is not easy to identify, strain  $\varepsilon_1$  corresponds to the intersection of the two lines with the slopes  $E_1$  and  $E_2$  (or  $E_1$  and  $E_3$  in the composites without the second stage). In this case,  $E_2$  (or  $E_3$ ) is evaluated based on the curve fitting in the second (or third) stage, which will be less than the slope of the first stage. As shown in Figure 1, in some inorganic matrix composites, the local rupture of the fibers at the third stage of the response leads to nonlinear behavior at this stage. In this case, slope  $E_3$  is obtained based on the linear response at the third stage.

### 3. Laboratory specimens

#### 3.1. Properties of materials

The inorganic matrix composite systems in this study consist of two main parts: fiber network and surrounding mortar. Two types of steel and glass fiber, together with two different types of inorganic lime and geopolymer mortars, were considered to evaluate the tensile behavior of the composites. The galvanized steel textile fiber network (coated with zinc) is constructed from the steel strands with a spacing of 6.35 mm (Figure 2(a)). Each of these strands is obtained by wrapping 2 wires

around three central wires (Figure 2(b)) and has a cross-sectional area of  $0.538 \text{ mm}^2$  [53].

The symmetrical glass fiber network is a coating of white Styrene-Butadiene Rubbers (SBRs) which has a resistance to alkaline media. As shown in Figure 3, the clearance between the fiber strands in this network is 17 mm and the cross-sectional area of each fiber strand is  $0.92 \text{ mm}^2$  [53].

In both steel and glass fiber networks, the strands of the longitudinal and transverse fibers are not attached together and are interwoven and clamped by means of small nylon fibers. The mechanical properties of the steel and glass fiber networks, along with their coefficients of variation, are presented in Table 1, and are obtained based on the results of tensile testing of the uncoated fibers by the manufacturer [53].

In this paper, the steel-fiber composites including 8 fibers are coated with two types of inorganic lime and geopolymer mortars and the glass-fiber composites including 3 fibers are only coated with the inorganic

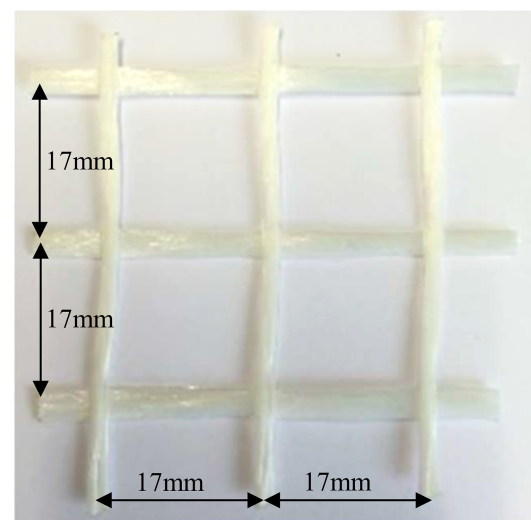


Figure 3. Textile glass fiber network.

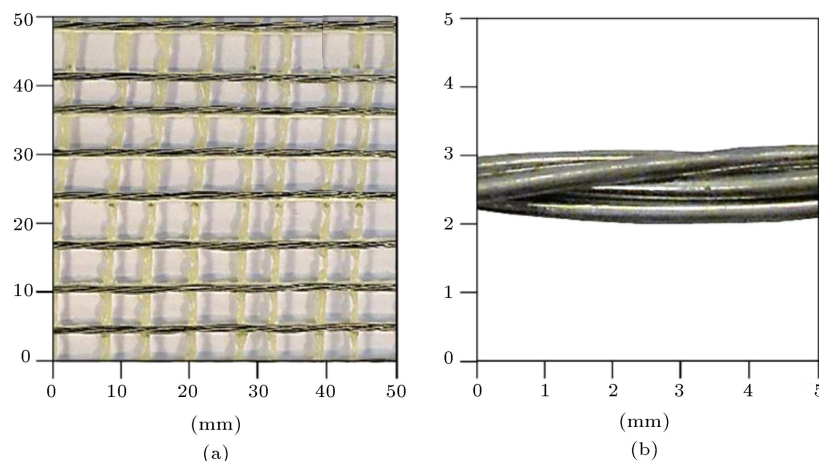


Figure 2. (a) Steel textile fiber network. (b) Details of a strand of steel fibers.

**Table 1.** Mechanical properties of steel and glass fiber networks reported by manufacturer [53].

Properties	Steel fibers	Glass fibers
Number of strands per mm (Transverse direction)	0.157	0.058
Tensile strength (MPa)	3191 (2%)*	1521 (4%)*
Modulus of elasticity (GPa)	186 (1%)*	149 (6%)*
Ultimate strain (%)	2.19 (3%)*	1.82 (2%)*
Equivalent thickness (mm)	0.084	0.056

\*: Coefficient of Variation (CoV) is presented in parentheses (%).

lime mortars. The lime (L) mortar consists of bauxite (aluminum hydroxide) binders and the geopolymer (P) mortar consists of geopolymer binders such as natural kaolin (aluminum silicate hydrate). The lime mortars are generally suitable for strengthening the historical substrates that require low elasticity to achieve the required mechanical properties, and the permeability coefficient are used to establish the maintenance criteria. On the other hand, the geopolymer (P) mortars are suitable for new building structures and infills, where expectation of additional loads to transfer is more important than permeability. Table 2 reports the mechanical properties of each mortar, including the compressive strength ( $f_{cm}$ ), tensile strength ( $f_{tm}$ ) and modulus of elasticity ( $E_{cm}$ ) along with their coefficient of variations. The mechanical properties of the mortars are presented based on the manufacturers' report [53].

### 3.2. Test setup

Tensile tests were performed to achieve the comprehensive characteristics of the inorganic matrix composites. The specimens considered for this tests were strips of 10 mm thickness (which are typically equal to the thickness of the inorganic matrix composites for strengthening the structures), 600 mm length and a constant width of 50 mm, which were constructed with flat aluminum and metal molds. In these molds, the first layer of the mortar was applied with a thickness of 5 mm, then, the steel or glass fiber network was placed in a longitudinal direction, and finally, the second layer of mortar coated the fiber network with a thickness of 5 mm. Each strip was individually

constructed rather than by cutting off a larger plate. The mold of specimens was opened after 2–3 days and kept wet up to 28 days, according to the manufacturer's suggestion [53]. Then, prior to the experiment, they were kept for 7 days under laboratory conditions. Prior to the experiment, the smoothness of specimens and the presence of shrinkage cracks were evaluated and inappropriate specimens were discarded. For the tensile tests, five specimens were selected for each of the inorganic matrix composites constructed from steel and glass fibers with lime mortar, and six specimens were selected for the inorganic matrix composite constructed from steel fibers with geopolymer mortar.

To prevent the fibers from slipping between the composite matrix and to obtain the fiber rupture at the end of the tensile tests, both ends of the specimen were clamped [54]. Using the compressive force of the device strokes, which applies to the matrix surrounding the fiber at both ends of the specimen, extends the mechanism of stress transfer between the fibers and the composite matrix, and makes it possible to achieve ultimate composite capacity in the tensile test by preventing the slip of the fiber within the matrix. However, the compressive force applied by the test device strokes on the specimens results in stress concentration at both ends of the composite and can cause specimen failure due to the crushing of the matrix between the clamps and the early failure of the specimen near and outside the clamped area [30]. Although many methods have been proposed in previous studies to prevent the crushing of the matrix between the tensile test device clamps [55], it still seems difficult to achieve a suitable method for preventing such failure. In addition, in most cases, clamping the beginning and end of the specimen during the tensile test of the inorganic matrix composite is not undertaken in operational applications, unless the reinforcement system is restrained at both ends by means of specific tools. Therefore, the parameters derived from the tensile tests using the clamping of both ends of the specimen should be used to achieve the composite properties and cannot be used without considering support conditions and consistency with actual applications in the design process.

In this paper, all specimens were reinforced with FRP sheets at both ends. Two layers of carbon FRP sheets, each with a thickness of 0.22 mm, coated a

**Table 2.** Mechanical properties of inorganic matrices [53].

Inorganic matrix	Notation	$f_{cm}$ (MPa)	$f_{tm}$ (MPa)	$E_{cm}$ (GPa)
Lime mortar	L	20.60 (4%)*	5.42 (4%)*	11.42 (5%)*
Geopolymer mortar	P	56.30 (3%)*	10.31 (3%)*	22.01 (8%)*

\*: Coefficient of Variation (CoV) is presented in parentheses (%).

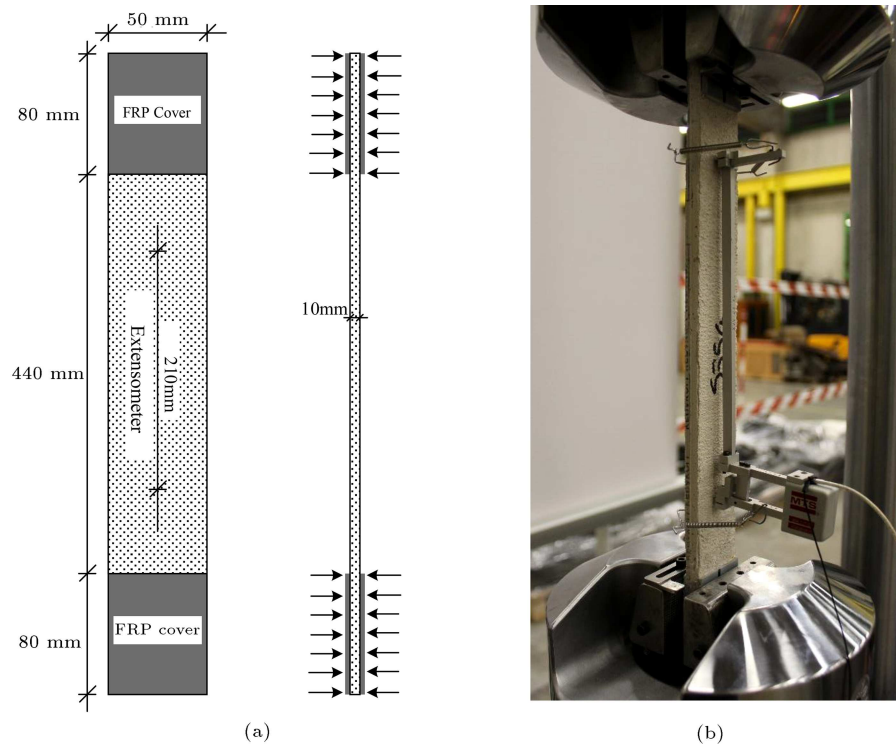


**Figure 4.** (a) Geometry of strip composites. (b) Tensile test setup (specimen T\_SL-1).

length of 80 mm length at both ends of each specimen. The test clamps applied a compressive force of 76 kN perpendicular to the surface of the specimens at both reinforced ends. This force resulted in a tensile stress of 21.10 MPa for the composites with a steel fiber network and 12.70 MPa for the composites with a glass fiber network. The compressive force of the device clamps was selected so that the resulting stress is consistent with the compressive strength of the composite matrix. Due to the reinforcement of the specimens at both ends using the FRP sheets, this stress is not expected to cause the specimen to be crushed at both ends. In this study, the extensometers, 210 mm in length, were used to measure the strains, which were placed in the middle of the specimen on the composite matrix. The extensometer is installed on the specimen by means of spring clamps to create the required friction with the specimen surface and, on the other hand, not to affect its behavior.

The amount of applied load is measured with the test device load cell and is divided by the cross-sectional area of the textile fiber network to achieve the stress. The convention for achieving the amount of stresses prevents the effect of composite thickness changes on the results, which is especially difficult to measure in practical tasks. The tests were conducted based on the displacement control of the device clamps at the loading rate of 0.01 m/s, based on a trial and error procedure. According to Figure 4, the displacement of specimens is measured using the LVDTs of the

test device in upper and lower strokes, which report the total displacement of the specimen. In addition, the extensometer placed on the outer layer of the mortar also provides a more accurate assessment of the displacements in the middle of the specimen. In accordance with the US AC 434 standard [56], the use of extensometers with a minimum length of 50 mm is sufficient to calibrate a particular crack. In this way, the extensometer used in this study, with a longitudinal coating of 210 mm and nearly one third of the specimen clearance, is suitable for measuring the strain field. The proposed average strains are calculated by dividing the amount of displacements measured by the extensometers by the covered length.

The specimens are given the notation of T\_XY\_N based on the type of fiber and inorganic matrix mortar, where T demonstrates the tensile test, X denotes the type of textile fiber (S for steel fibers and G for glass fibers), Y represents the type of mortar used in the composite (L for lime mortar and P for geopolymer mortars), and N is the special number for each specimen.

#### 4. Test results

##### 4.1. Load-displacement and axial stress-strain diagrams

The results of the tensile tests in the form of load-displacement and axial stress-strain diagrams are shown for the steel-fiber composites coated with lime

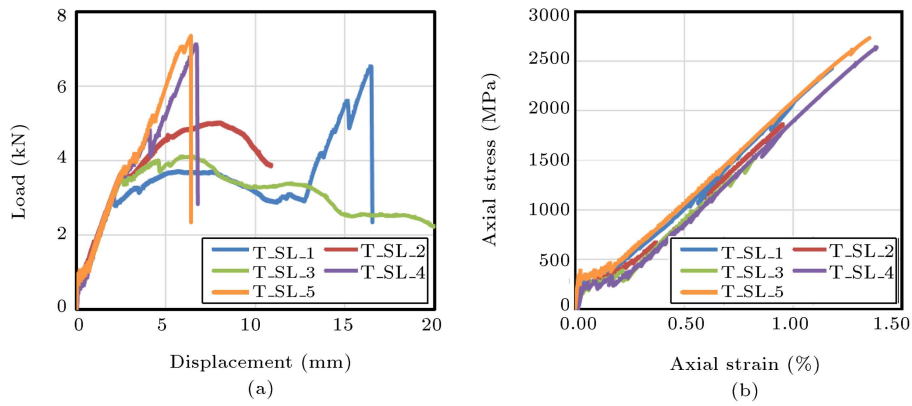


Figure 5. (a) Axial load-displacement diagrams, and (b) axial stress-strain diagrams in SL group of composites.

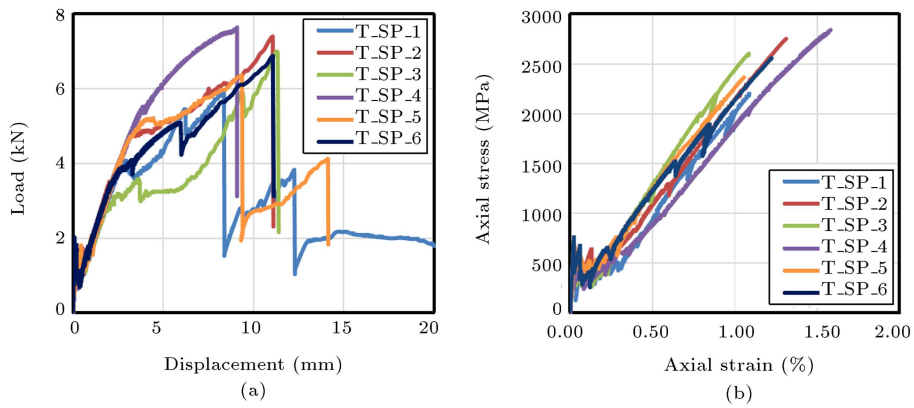


Figure 6. (a) Axial load-displacement diagrams, and (b) axial stress-strain diagrams in SP group of composites.

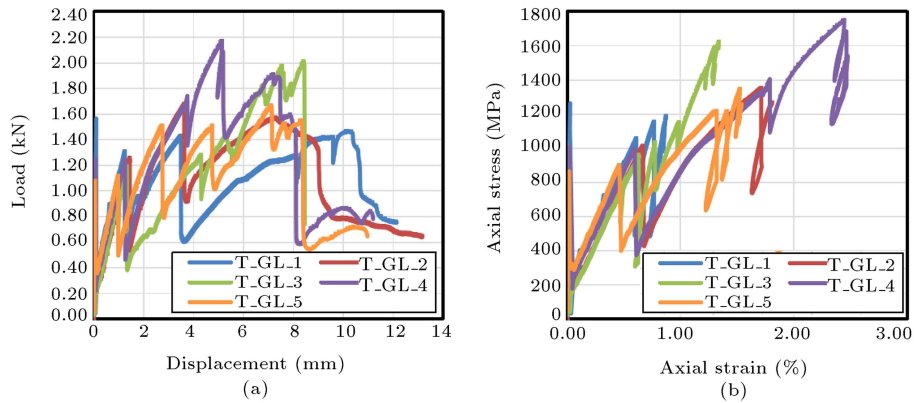


Figure 7. (a) Axial load-displacement diagrams, and (b) axial stress-strain diagrams in GL of composites.

mortar (SL group) in Figure 5, for the steel-fiber composites coated with geopolymer mortar (SP group) in Figure 6, and for the glass fiber composites coated with lime mortar (GL group) in Figure 7. Due to the fact that the extensometers are removed from the specimen before the ultimate failure to prevent damage, the slip shown in the load-displacement diagrams is not seen in the stress-strain diagrams of the specimens.

The axial load-displacement diagrams and, consequently, the stress-strain diagrams obtained from the tensile tests of inorganic matrix composite specimens,

Figures 5 to 7, can be summarized in some parameters. Table 3 shows the parameters resulting from the stress-strain diagrams of specimens, including the stresses and strains related to points  $T_1$  and  $T_2$ ,  $\sigma_{T1}$ ,  $\varepsilon_{T1}$ ,  $\sigma_{T2}$ ,  $\varepsilon_{T2}$ , the maximum stress and corresponding strain,  $\sigma_{max}$ ,  $\varepsilon_{max}$ , the elasticity modulus of all three stages,  $E_1$ ,  $E_2$  and  $E_3$ , and finally, the Failure Mode (FM) of the specimen.

All the stresses presented in Table 3 are calculated by dividing the applied load by the fiber network cross-section (equal to  $2.69 \text{ mm}^2$  for SL and SP groups

**Table 3.** Direct tensile test results on composite specimens of SL, SP, and GL groups.

Specimen		Stage I			Stage II			Stage III			Cracks		FM
Group	Name	$\sigma_{T1}$ (MPa)	$\varepsilon_{T1}$ (%)	$E_1$ (GPa)	$\sigma_{T2}$ (MPa)	$\varepsilon_{T2}$ (%)	$E_2$ (GPa)	$\sigma_{max}$ (MPa)	$\varepsilon_{max}$ (%)	$E_3$ (GPa)	$d$ (mm)	$n$	
SL	T_SL_1	301	0.0205	1487	255	0.0815	—	2426	1.1774	210	29	14	A-C
	T_SL_2	201	0.0124	1607	383	0.1928	—	1854	0.9519	207	25	16	C
	T_SL_3	300	0.0135	2156	286	0.2197	—	1524	0.8262	199	22	19	C
	T_SL_4	223	0.0292	1924	236	0.1743	—	2617	1.3763	205	25	16	C
	T_SL_5	383	0.0238	2369	378	0.1627	—	2734	1.3498	201	23	18	A-C
	Average	282	0.0198	1909	307	0.1662	—	2231	1.1363	204	24.8	16	—
	CoV (%)	25.7	35.6	19.3	22.4	31.3	—	23.3	21.4	2.1	10.82	11	—
SP	T_SP_1	529	0.0163	3383	496	0.2882	—	2187	1.0873	218	26	16	A
	T_SP_2	513	0.0155	3254	520	0.2401	—	2753	1.3116	212	27	15	A
	T_SP_3	723	0.0207	3486	464	0.2299	—	2585	1.0836	255	36	11	A
	T_SP_4	521	0.0207	3585	475	0.2114	—	2842	1.5818	182	34	12	A
	T_SP_5	668	0.0258	3183	584	0.2028	—	2365	1.0555	218	35	12	A
	T_SP_6	752	0.0226	3283	645	0.2271	—	2558	1.2235	193	29	14	C
	Average	618	0.0203	3362	531	0.2332	—	2548	1.2239	213	31.17	13	—
CoV (%)	17.7	19.2	4.5	13.2	12.8	—	9.5	16.4	11.8	13.97	14	—	
GL	T_GL_1	1258	0.0246	5927	208	0.0485	—	1180	0.8712	145	43	9	B
	T_GL_2	897	0.0182	5025	161	0.0279	—	1265	1.8067	137	39	10	C
	T_GL_3	818	0.0159	5078	149	0.0329	—	1585	1.3344	134	41	10	A
	T_GL_4	1002	0.0176	5494	205	0.0455	—	1751	2.4416	139	47	8	A-C
	T_GL_5	863	0.0162	5133	288	0.0605	—	1345	1.5226	152	38	11	A
	Average	968	0.0185	5331	202	0.0431	—	1425	1.5953	141	41.6	10	—
	CoV (%)	18.2	19.3	7.1	27.1	30.2	—	16.6	36.5	5.1	8.61	11	—

and 2.76 mm<sup>2</sup> for GL group of composites). All of the strains provided in Table 3 are also derived from the division of the displacements measured by the extensometer by its length, 210 mm.

The evaluation of the stress-strain diagrams in Figures 5(b) and 6(b) and their resulting parameters in Table 3 for the composites of SL and SP groups shows that the first and second stages are well visible for the stronger mortars, geopolymers, and the amount of stress  $\sigma_{T1}$ , stress at the end of the first stage, has higher values. According to Table 3, the average stress  $\sigma_{T1}$  relative to the average tensile strength for the SL group of composites is 12.6% and for the SP group of composites is 24.3%. At the end of the first stage, the SP group composites exhibit a higher drop in stresses compared to the SL group composites. In contrast, the amount of mortar strength was lower in

the SL group composites and the contribution of the specimens in the first and second stages of the response was lower. This can be attributed to the lower level of bonding between the fibers and mortars with weaker mechanical properties.

The analysis of the results in Table 3 shows that the parameters derived from the first and second stages are very scattered for all the inorganic matrix composites. The frequency of stress variation coefficients in the first and second stages,  $\sigma_{T1}$  and  $\sigma_{T2}$ , and the corresponding strains,  $\varepsilon_{T1}$  and  $\varepsilon_{T2}$ , represents such scattering. In the case of first stage, this scattering is explained by the fact that the parameters of this stage depend on the overall cross-section of the composite, while the presented mechanical properties are calculated based on the fiber cross-section. In addition, changing the way the cracks are developed in

the specimens in the second phase caused the scattering of the responses. The results can also be affected by the conditions for the construction and maintenance of the specimens and the development of cracks in the specimen prior to the tensile test due to the shrinkage or when the specimen is placed in the test device. The presence of micro-cracks, particularly in the GL group of composite specimens, does not allow appropriate redistribution of the load between the different strands of glass fiber, and as a result, causes the early failure of the specimen and ultimate capacity is not achieved due to successive ruptures in the fibers. The successive drops in the third stage of the axial stress-strain diagrams of the GL group composite specimens indicate the inappropriate redistribution of the load between the strands of glass fiber and their successive rupture.

In general, the tensile strength of the inorganic matrix composite,  $\sigma_{\max}$ , is different from the results obtained from the tensile test of textile fibers (Table 1) by 30.1% for the SL group of composites, 20.2% for the SP group of composites, and 6.3% for the GL group of composites. The reason for this difference can be attributed to the uneven redistribution of the load between the different strands of the fiber and also the slip of the fiber between the inorganic matrix layers of the composite due to the development of micro-cracks. The elasticity modules at the final stage of the tensile tests of the composites are consistent with a difference of 9.6% for the SL group of composites, 14.5% for the SP group of composites, and 5.4% for the GL group of composites from the elastic modules reported for the bare steel and glass fibers in Table 1. Finally, due to the increased stiffness of the mortar in the composites at the first stage of the tensile test, the maximum strain of the composites was decreased by 48.1% for GL specimens, 44.2% for the SL group of composites, and 12.3% for the SP group of composites compared to the maximum strain of textile fibers.

Regarding the obtained results presented in Table 3, the ductility values, average  $\varepsilon_{\max}$  to  $\varepsilon_{T1}$  ratio, of the SL, SP and GL groups of composites are 57.39, 60.29 and 86.23, respectively, which are calculated as

being higher in the glass fiber reinforced specimens, as compared to the steel ones.

#### 4.2. Failure Modes (FM)

As shown in Figure 8, the FM of inorganic matrix composites in tensile tests can be classified into three groups [41]: rupture of fibers in a major crack near the clamped part at both ends of the specimen, failure mode A (Figure 8(a)), rupture of fibers in a major crack in the middle part of the specimen, failure mode B (Figure 8(b)), and opening of a major crack close to the clamped part of the specimen with the slip of the fibers, failure mode C (Figure 8(c)). However, the combined FM can occur as the rupture of some fibers and the slip of some other fibers.

There is a random location for the occurrence of a major crack in the specimen leading to its failure. However, when the specimen clamping method is used for the tensile test, the stress concentration at both ends of the specimen causes the opening of major cracks close to the clamped area. When, due to the opening of major cracks near both ends of the specimen, the fibers slip within the composite matrix, failure mode C, the amount of tensile strength of the specimen is lower compared with the mode where the failure of the specimen occurs due to the rupture of the fiber, failure modes A and B. Therefore, for the tensile test device that uses the clamping of both ends of the specimen, the tensile strengths obtained from the specimens with failure mode C should not be evaluated.

When a major crack opens, the fibers located between the two edges of the crack resist all the applied load, and their rupture causes the specimen to fail. Therefore, the clamping pressure at both ends of the specimen should not be linked to the rupture of the fibers between the two edges, which may result in the development of a major crack near the clamped area. It should be noted that cracks in the matrix of the composites typically occur both inside and outside the region coated by the extensometer. Hence, the measured strains do not always reflect the overall behavior of the studied specimen. However, due to the consistency of the results obtained from specimens that

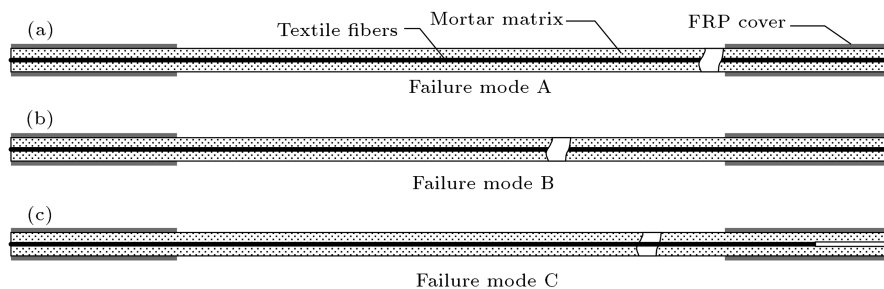


**Figure 8.** Different Failure Modes (FM) in tensile test on inorganic matrix composite specimens: (a) Failure mode A, (b) failure mode B, and (c) failure mode C.

have cracks outside the extensometer region, and those with intermediate cracks, the general axial stress-strain behavior of the specimens can be expressed using the strains measured by the extensometers.

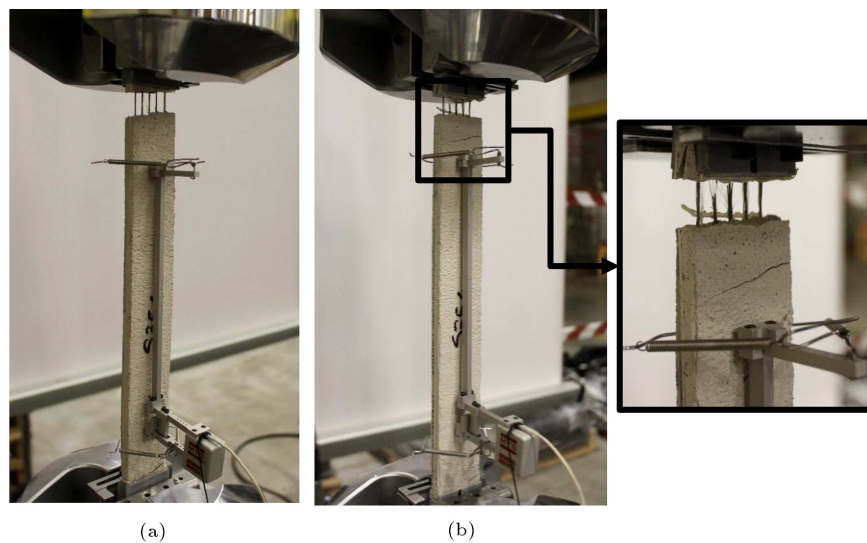
The FM of the SL group strip composites are shown in Figure 9. Failure in most specimens of this group was the development of major cracks near the clamped region at both ends of the specimen, along with the slip of the fibers within the composite matrix, failure mode C. In other specimens of this group, failure occurred as the rupture of some fibers and the slip of some other fibers, combined failure mode A–C. The slip of the fibers within the composite matrix, which has been reported in previous studies for various inorganic matrix composites reinforced with steel fibers [38], can be attributed to the inconsistency of the mechanical properties of the fibers and the matrix (strong textile fibers versus a low-durability matrix) and the application of insufficient clamping force (approximately 76 kN) that could not prevent the fibers from slipping. However, the obtained  $E_3$  values are consistent with the elasticity modulus of the bare steel fibers resulting from the tensile test of the fiber strands. This indicates that the clamping method used in this study allowed the composite properties to be achieved until failure mode C.

Although a large number of cracks were developed along the specimens before failure of the specimen of SL group composites, there is no sharp drop in the stress-strain curve. This suggests the minor role of the composite matrix in resisting loads after the first stage. The amount of clamping stress applied by the test device clamps is equal to 21 MPa, which is slightly higher than the compressive strength of the lime mortar used in the composites of this group (20.60 MPa

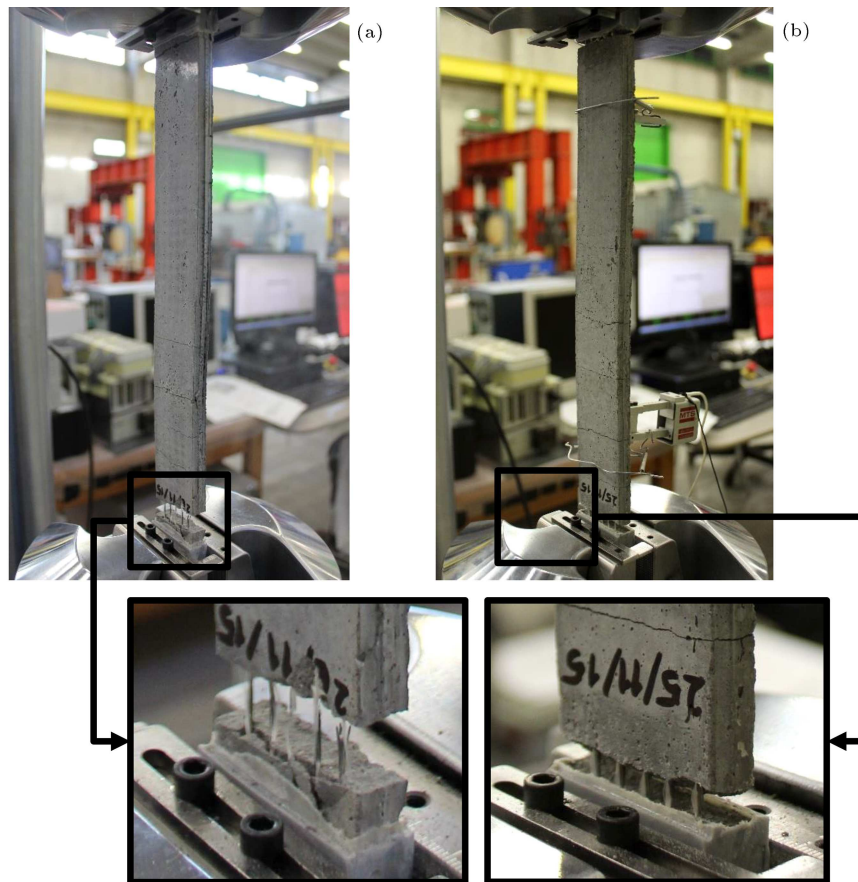
according to Table 2). Although the presence of FRP coatings on both ends of the specimen increases the compressive strength of the matrix, by restricting the transverse strains at both ends of the composite, the increased clamping stresses may cause the matrix to crack between the clamps. This could reduce the matrix contribution in the response of the specimens (decrease in stresses  $\sigma_{T1}$ ) and increase the possibility of fiber slipping within the composite matrix.

Figure 10 shows the different FM in the specimen of the SP group strip composites. In contrast to the SL group composites, most SP group specimens experienced rupture of the fibers in a major crack near the clamped region at both ends of the specimen, failure mode A. Among all the specimens in this group, failure mode C was only observed in the T.SP-6 specimen.

Comparison of the FM of strip composite specimens in SL and SP groups shows that the geopolymer mortars used in the SP group were capable of more appropriately coating the fibers compared with the lime mortars used in the SL group. Therefore, by preventing the slip of the fibers in the inorganic matrix, the common FM in the SP group specimens was the rupture of the fibers near both ends of the specimen. In these specimens, due to the fact that the fibers within the inorganic matrix do not slip, the number of cracks developed along the specimens prior to failure is higher compared with the specimen of the SL group of composites. In addition, based on the results reported in Table 3, the average stresses at the end of the first, second and third stages in the stress-strain curve,  $\sigma_{T1}$ ,  $\sigma_{T2}$  and  $\sigma_{max}$ , in the composite specimens of the SP group are 119.1%, 72.9% and 14.2% higher compared with the composite specimens of the SL



**Figure 9.** Failure Modes (FM) in composite specimens of SL group: (a) Failure mode C in specimen T\_SL-3, and (b) failure mode A–C in specimen T\_SL-1.



**Figure 10.** Failure modes in composite specimens of SP group: (a) Failure mode A in specimen T\_SP\_5, and (b) failure mode C in specimen T\_SP\_6.

group, respectively. In the specimens of the SP group, the average values of strains at the end of the first and second stages,  $\varepsilon_{T1}$ ,  $\varepsilon_{T2}$ , were 2.5% and 40.3% higher compared with the SL group, and despite the slip of the fibers, the average ultimate strain,  $\varepsilon_{max}$ , is 7.7% higher, respectively.

The FM of the strip composite specimens in the GL group are shown in Figure 11. The low density of glass fibers in this group and the low tensile strength of the fibers and the surrounding lime mortar resulted in rupture of the fibers in a different order and caused different types of FM. In one specimen of this group, specimen T\_GL\_1, the rupture of the fibers occurred in the middle part of the specimen, failure mode B; in the other one, specimen T\_GL\_2, the opening of a major crack close to the clamped region of the specimen occurred with the fiber slip, failure mode C; and in the other specimens, failure mode A occurred combined with failure mode C, failure mode A–C.

In the GL group composite specimens, the low density of the glass-fiber network caused the lime matrix to fully coat the fibers. Hence, in comparison with the composite specimens of SL and SP groups, they have higher average stresses  $\sigma_{T1}$  and elasticity modulus  $E_1$ . On the other hand, the presence of microcracks

in the specimens of this group does not allow the appropriate redistribution of the load between different strands of glass fiber. As a result, consistent with the successive drops observed in the stress-strain diagrams of these specimens, the successive rupture in the fibers in the specimens of this group results in their early failure and in not achieving ultimate capacity.

In order to better compare different FRIM systems and to investigate the effects of mortar type on tensile behavior, the number ( $n$ ) and distance ( $d$ ) of cracks are reported in Table 3. The results show that, consistent with different FM, the average number of cracks in SL, SP and GL groups of composites are 16, 13 and 10, respectively.

## 5. Conclusion

In this paper, to understand the tensile behavior of inorganic matrix composites, an experimental study of this behavior was conducted for two types of steel and glass fiber. The composites constructed from steel fibers were coated with two types of inorganic lime and geopolymer mortars (SL and SP, respectively) and the glass-fiber composites were only coated with the inorganic lime mortars (GL). To achieve the final

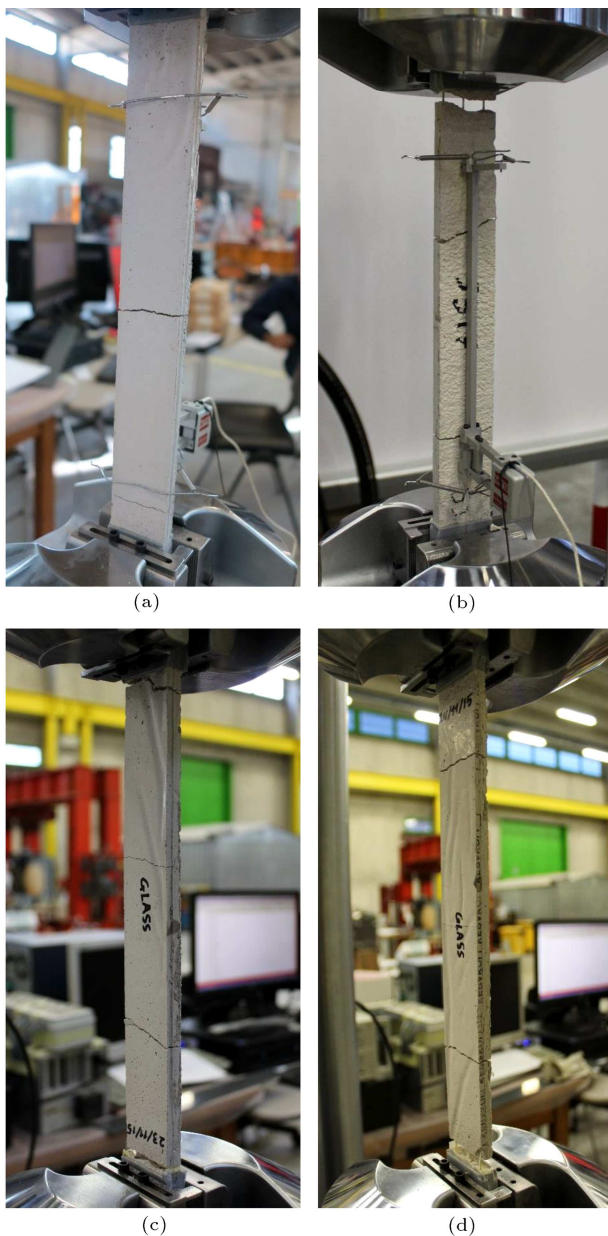


**Figure 11.** Failure modes in composite specimens of GL group: (a) Failure mode B in specimen T\_GL-1, (b) failure mode C in specimen T\_GL-2, (c) failure mode A in specimen T\_GL-3, and (d) failure mode A–C in specimen T\_GL-4.

response stage in the tensile test of the composites, the specimens were clamped on the mortar by applying adequate compressive force to prevent the slip of the fibers within the surrounding mortar. The strains, stresses and crack spacing were also measured by means of the extensometers placed in the middle of the specimen on the mortar. The following results were obtained from the tensile tests:

- The presence of microcracks, particularly in the GL group composite specimen, does not allow the appropriate redistribution of the load between the

different strands of the glass fiber, and as a result, causes the early failure of the specimen and non-achievement of ultimate capacity by the successive ruptures in the fibers;

- The tensile strength of the inorganic matrix composite is different from the results obtained from the tensile test of textile fibers without the coating by 30.1% for the SL group of composites, 20.2% for the SP group of composites, and 6.3% for the GL group of composites. The reason for this difference can be attributed to the uneven redistribution of the load between the different strands of the fiber and also the slip of the fiber between the inorganic matrix layers of the composite due to the development of microcracks;
- The elasticity modulus at the final stage of the tensile tests of the composites are consistent, with a difference of 9.6% for the SL group of composites, 14.5% for the SP group of composites, and 5.4% for the GL group of composites, from the elastic modulus reported for the bare steel and glass fibers;
- Due to the increased stiffness of the mortar in the composites in the first stage of the tensile test, the maximum strain of the composites was decreased 48.1% for GL specimens, 44.2% for the SL group of composites, and 12.3% for the SP group of composites compared to the maximum strain of textile fibers;
- Failure in most specimens of the SL group was the development of major cracks near the clamped region at both ends of the specimen, along with the slip of fibers within the composite matrix. In other specimens of this group, the failure occurred as the rupture of some fibers and the slip of some other fibers. In contrast to the SL group of composites, most SP group specimens experienced rupture of the fibers in a major crack near the clamped region at both ends of the specimen;
- The low density of glass fibers in the strip composites of the GL group and also the low tensile strength of the fibers and the surrounding lime mortar resulted in fiber rupture in a different order and caused different types of failure mode.

### Acknowledgements

The authors convey sincere gratitude to Dr. Christian Carloni, as well as the technicians of LISG (Laboratory of Structural and Geotechnical Engineering) and CIRI (Interdepartmental Centre for Industrial Research in Building and Construction) for sharing their knowledge and experience throughout this research during the first author's sabbatical leave at the University of Bologna, Italy. The authors also greatly appreciate

the assistance of Kerakoll S.P.A., Italy, for providing composite materials for testing.

## References

1. Bagheri, M., Chahkandi, A., and Jahangir, H. "Seismic reliability analysis of RC frames rehabilitated by glass fiber-reinforced polymers", *Int. J. Civ. Eng.*, **17**(11), pp. 1785–1797 (2019).
2. Kouris, L.A.S. and Triantafillou, T.C. "State-of-the-art on strengthening of masonry structures with textile reinforced mortar (TRM)", *Constr. Build. Mater.*, **188**, pp. 1221–1233 (2018).
3. Jahangir, H. and Esfahani, M.R. "Investigating loading rate and fibre densities influence on SRG - concrete bond behaviour", *Steel Compos. Struct.*, **34**(6), pp. 877–889 (2020).
4. Parisi, F., Menna, C., and Prota, A. "Fabric-Reinforced Cementitious Matrix (FRCM) composites", In *Failure Analysis in Biocomposites, Fibre-Reinforced Composites and Hybrid Composites*, Elsevier, pp. 199–227 (2019).
5. D'Ambrisi, A., Feo, L., and Focacci, F. "Experimental analysis on bond between PBO-FRCM strengthening materials and concrete", *Compos. Part B Eng.*, **44**(1), pp. 524–532 (2013).
6. Ombres, L. "Analysis of the bond between Fabric Reinforced Cementitious Mortar (FRCM) strengthening systems and concrete", *Compos. Part B Eng.*, **69**, pp. 418–426 (2015).
7. Santandrea, M., Imohamed, I.A.O., Jahangir, H., Carloni, C., Mazzotti, C., De Miranda, S., Ubertini, F., and Casadei, P. "An investigation of the debonding mechanism in steel FRP- and FRCM-concrete joints", *4th Work. New Boundaries Struct. Concr.*, Capri Island, Italy, pp. 289–298 (2016).
8. Jahangir, H. and Esfahani, M.R. "Numerical study of bond-slip mechanism in advanced externally bonded strengthening composites", *KSCCE J. Civ. Eng.*, **22**(11), pp. 4509–4518 (2018).
9. Mazzuca, S., Hadad, H.A., Ombres, L., and Nanni, A. "Mechanical characterization of steel-reinforced grout for strengthening of existing masonry and concrete structures", *J. Mater. Civ. Eng.*, **31**(5), p. 04019037 (2019).
10. Babaeidarabad, S., Loreto, G., and Nanni, A. "Flexural strengthening of RC beams with an externally bonded fabric-reinforced cementitious matrix", *J. Compos. Constr.*, **18**(5), p. 4014009 (2014).
11. Jiang, S., Guo, X., Xiong, Z., Cai, Y., and Zhu, S. "Experimental studies on behaviour of tubular T-joints reinforced with grouted sleeve", *Steel Compos. Struct.*, **23**(5), pp. 585–596 (2017).
12. Jahangir, H. and Esfahani, M.R. "Strain of newly - developed composites relationship in flexural tests (in Persian)", *J. Struct. Constr. Eng.*, **5**(3), pp. 92–107 (2018).
13. Thermou, G.E., Papanikolaou, V.K., Lioupis, C., and Hajirasouliha, I. "Steel-Reinforced Grout (SRG) strengthening of shear-critical RC beams", *Constr. Build. Mater.*, **216**, pp. 68–83 (2019).
14. Alabdulhady, M.Y. and Sneed, L.H. "Torsional strengthening of reinforced concrete beams with externally bonded composites: A state of the art review", *Constr. Build. Mater.*, **205**, pp. 148–163 (2019).
15. Strauss Rambo, D.A., de Andrade Silva, F., Toledo Filho, R.D., Ukrainczyk, N., and Koenders, E. "Tensile strength of a calcium-aluminate cementitious composite reinforced with basalt textile in a high-temperature environment", *Cem. Concr. Compos.*, **70**, pp. 183–193 (2016).
16. Leone, M., Aiello, M.A., Balsamo, A., Carozzi, F.G., Ceroni, F., Corradi, M., Gams, M., Garbin, E., Gattesco, N., Krajewski, P., Mazzotti, C., Oliveira, D., Papanicolaou, C., Ranocchiai, G., Roscini, F., and Saenger, D. "Glass fabric reinforced cementitious matrix: Tensile properties and bond performance on masonry substrate", *Compos. Part B Eng.*, **127**, pp. 196–214 (2017).
17. Jesse, F., Schicktzan, K., and Curbach, M. "Obtaining characteristic material strength of Textile Reinforced Concrete (TRC) from laboratory tests", *Proc. 9th Int. Symp. Ferrocem. (Ferro9)*, Bali, pp. 305–318 (2009).
18. Carozzi, F.G., Milani, G., and Poggi, C. "Mechanical properties and numerical modeling of Fabric Reinforced Cementitious Matrix (FRCM) systems for strengthening of masonry structures", *Compos. Struct.*, **107**, pp. 711–725 (2014).
19. De Santis, S., Carozzi, F.G., de Felice, G., and Poggi, C. "Test methods for Textile Reinforced Mortar systems", *Compos. Part B Eng.*, **127**, pp. 121–132 (2017).
20. Ferrara, G., Coppola, B., Di Maio, L., Incarnato, L., and Martinelli, E. "Tensile strength of flax fabrics to be used as reinforcement in cement-based composites: experimental tests under different environmental exposures", *Compos. Part B Eng.*, **168**, pp. 511–523 (2019).
21. Contamine, R., Si Larbi, A., and Hamelin, P. "Contribution to direct tensile testing of textile reinforced concrete (TRC) composites", *Mater. Sci. Eng. A*, **528**(29–30), pp. 8589–8598 (2011).
22. Carozzi, F.G. and Poggi, C. "Mechanical properties and debonding strength of Fabric Reinforced Cementitious Matrix (FRCM) systems for masonry strengthening", *Compos. Part B Eng.*, **70**, pp. 215–230 (2015).
23. Caggegi, C., Lanoye, E., Djama, K., Bassil, A., and Gabor, A. "Tensile behaviour of a basalt TRM strengthening system: Influence of mortar and reinforcing textile ratios", *Compos. Part B Eng.*, **130**, pp. 90–102 (2017).
24. Bellini, A., Bovo, M., and Mazzotti, C. "Experimental and numerical evaluation of fiber-matrix interface behaviour of different FRCM systems", *Compos. Part B Eng.*, **161**, pp. 411–426 (2019).

25. Papantoniou, I.C. and Papanicolaou, C.G. “Flexural behavior of one-way textile reinforced concrete (TRC)/reinforced concrete (RC) composite slabs”, *15TH Eur. Conf. Compos. Mater.*, Venice, Italy (2012).
26. Tosun-Felekoğlu, K., Felekoğlu, B., Ranade, R., Lee, B.Y., and Li, V.C. “The role of flaw size and fiber distribution on tensile ductility of PVA-ECC”, *Compos. Part B Eng.*, **56**, pp. 536–545 (2014).
27. D’Antino, T. and Papanicolaou, C. “Comparison between different tensile test set-ups for the mechanical characterization of inorganic-matrix composites”, *Constr. Build. Mater.*, **171**, pp. 140–151 (2018).
28. Li, B., Xiong, H., Jiang, J., and Dou, X. “Tensile behavior of basalt textile grid reinforced Engineering Cementitious Composite”, *Compos. Part B Eng.*, **156**, pp. 185–200 (2019).
29. Caggegi, C., Carozzi, F.G., De Santis, S., Fabbrocino, F., Focacci, F., Hojdys, L., Lanoye, E., and Zuccarino, L. “Experimental analysis on tensile and bond properties of PBO and aramid fabric reinforced cementitious matrix for strengthening masonry structures”, *Compos. Part B Eng.*, **127**, pp. 175–195 (2017).
30. Pellegrino, C. and D’Antino, T. “Experimental behaviour of existing precast prestressed reinforced concrete elements strengthened with cementitious composites”, *Compos. Part B Eng.*, **55**, pp. 31–40 (2013).
31. Donnini, J. and Corinaldesi, V. “Mechanical characterization of different FRCM systems for structural reinforcement”, *Constr. Build. Mater.*, **145**, pp. 565–575 (2017).
32. Ascione, L., de Felice, G., and De Santis, S. “A qualification method for externally bonded Fibre Reinforced Cementitious Matrix (FRCM) strengthening systems”, *Compos. Part B Eng.*, **78**, pp. 497–506 (2015).
33. Arboleda, D., Carozzi, F.G., Nanni, A., and Poggi, C. “Testing procedures for the uniaxial tensile characterization of fabric-reinforced cementitious matrix composites”, *J. Compos. Constr.*, **20**(3), p. 04015063 (2016).
34. Donnini, J., Corinaldesi, V., and Nanni, A. “Mechanical properties of FRCM using carbon fabrics with different coating treatments”, *Compos. Part B Eng.*, **88**, pp. 220–228 (2016).
35. Bernardi, P., Cerioni, R., Ferretti, D., Leurini, F., and Michelini, E. “Experimental characterization of fiber-reinforced cementitious mortar under tension”, *Frat. ed Integrità Strutt.*, **13**(48), pp. 97–104 (2019).
36. Dugas, M., Weise, S., Curbach, M., Hempel, R., Offermann, P., and Franzke, G. “Force-deformation behaviour of tensile-loaded specimen made of textile reinforced concrete”, *Text. Constr.*, **1**, pp. 143–152 (1998).
37. Contamine, R., Larbi, A.S., and Hamelin, P. “Contribution to direct tensile testing of textile reinforced concrete (TRC) composites”, *Mater. Sci. Eng. A*, **528**(29), pp. 8589–8598 (2011).
38. De Santis, S. and de Felice, G. “Tensile behaviour of mortar-based composites for externally bonded reinforcement systems”, *Compos. Part B Eng.*, **68**, pp. 401–413 (2015).
39. Cevallos, O.A. and Olivito, R.S. “Effects of fabric parameters on the tensile behaviour of sustainable cementitious composites”, *Compos. Part B Eng.*, **69**, pp. 256–266 (2015).
40. De Santis, S., Ceroni, F., de Felice, G., Fagone, M., Ghiassi, B., Kwiecień, A., Lignola, G.P., Morganti, M., Santandrea, M., Valluzzi, M.R., and Viskovic, A. “Round robin test on tensile and bond behaviour of steel reinforced grout systems”, *Compos. Part B Eng.*, **127**, pp. 100–120 (2017).
41. Carozzi, F.G., Bellini, A., D’Antino, T., de Felice, G., Focacci, F., Hojdys, L., Laghi, L., Lanoye, E., Micelli, F., Panizza, M., and Poggi, C. “Experimental investigation of tensile and bond properties of Carbon-FRCM composites for strengthening masonry elements”, *Compos. Part B Eng.*, **128**, pp. 100–119 (2017).
42. Saidi, M. and Gabor, A. “Use of distributed optical fibre as a strain sensor in textile reinforced cementitious matrix composites”, *Measurement*, **140**, pp. 323–333 (2019).
43. De Santis, S. and de Felice, G. “Steel reinforced grout systems for the strengthening of masonry structures”, *Compos. Struct.*, **134**, pp. 533–548 (2015).
44. Hartig, J., Jesse, F., Schick Tanz, K., and Häußler-Combe, U. “Influence of experimental setups on the apparent uniaxial tensile load-bearing capacity of textile reinforced concrete specimens”, *Mater. Struct.*, **45**(3), pp. 433–446 (2012).
45. Kim, H., Kim, G., Lee, S., Son, M., Choe, G., and Nam, J. “Strain rate effects on the compressive and tensile behavior of bundle-type polyamide fiber-reinforced cementitious composites”, *Compos. Part B Eng.*, **160**, pp. 50–65 (2019).
46. D’Antino, T. and Papanicolaou, C. “Mechanical characterization of textile reinforced inorganic-matrix composites”, *Compos. Part B Eng.*, **127**, pp. 78–91 (2017).
47. Al-Gemeel, A.N., Zhuge, Y., and Youssf, O. “Experimental investigation of basalt textile reinforced engineered cementitious composite under apparent hoop tensile loading”, *J. Build. Eng.*, **23**, pp. 270–279 (2019).
48. Signorini, C., Nobili, A., and Falope, F.O. “Mechanical performance and crack pattern analysis of aged Carbon Fabric Cementitious Matrix (CFRCM) composites”, *Compos. Struct.*, **202**, pp. 1114–1120 (2018).
49. Donnini, J., Chiappini, G., Lancioni, G., and Corinaldesi, V. “Tensile behaviour of glass FRCM systems

- with fabrics' overlap: Experimental results and numerical modeling", *Compos. Struct.*, **212**, pp. 398–411 (2019).
50. Hegger, J., Will, N., Curbach, M., and Jesse, F. "Tragverhalten von textiltbewehrtem Beton", *Beton- und Stahlbetonbau*, **99**(6), pp. 452–455 (2004).
  51. Hartig, J., Jesse, F., Schick Tanz, K., and Häußler-Combe, U. "Influence of experimental set ups on the apparent uniaxial tensile load-bearing capacity of textile reinforced concrete specimens", *Mater. Struct.*, **45**(3), pp. 433–446 (2012).
  52. Li, V. "Engineered Cementitious Composites (ECC) Material, Structural, and Durability Performance", In *Concrete Construction Engineering Handbook*, Nawy, E.G., Ed., CRC Press: Boca Raton, FL, USA, pp. 34–47 (2008).
  53. "Kerakoll S.p.A.", [www.kerakoll.com](http://www.kerakoll.com).
  54. Carozzi, F.G. and Poggi, C. "Mechanical properties and debonding strength of Fabric Reinforced Cementitious Matrix (FRCM) systems for masonry strengthening", *Compos. Part B Eng.*, **70**, pp. 215–230 (2015).
  55. Carozzi, F.G., Bellini, A., D'Antino, T., de Felice, G., Focacci, F., Hojdys, L., Laghi, L., Lanoye, E., Micelli, F., Panizza, M., and Poggi, C. "Experimental investigation of tensile and bond properties of Carbon-FRCM composites for strengthening masonry elements", *Compos. Part B Eng.*, **128**, pp. 100–119 (2017).
  56. AC434, I.C.C. "Proposed acceptance criteria for masonry and concrete strengthening using fiber-reinforced cementitious matrix (FRCM) composite systems", *ICC-Evaluation Serv.*, Whittier, CA (2013).

## Biographies

**Hashem Jahangir** is a Research Assistant in the Department of Civil Engineering at Ferdowsi University of Mashhad, Iran. He completed a long-term sabbatical leave at the University of Bologna in 2016, working on newly developed composite materials. His research interests include structural strengthening, structural health monitoring and damage detection in civil engineering.

**Mohammad Reza Esfahani** is Professor in the Department of Civil Engineering at Ferdowsi University of Mashhad, Iran. His research interests mainly include strengthening reinforced concrete elements, reinforced concrete structures analysis and concrete technology. He has published many papers in reputable journals and international conference proceedings.